Research Article

Electrodeposition and characterization of NiCoP

Kanchan Mondal[1] · Noppodan Sathithsuksanoh[2] · Shashi B. Lalvani[3]

Received: 17 January 2020 / Accepted: 19 November 2020

Abstract
The influence of the mass transfer effects, the applied current density, the solution pH and temperature, and bath composition on the current efficiency of the deposit was determined. Cyclic voltammetry on the deposition bath was conducted to understand the mechanism of deposition. The films were characterized by x-ray diffraction spectroscopy and were found to be generally amorphous with small amounts of crystalline phases dispersed depending upon the phosphorous content. The corrosion resistance of the deposits in a chloride medium was observed to increase with the phosphorous content. The knoop hardness of the electrodeposits was studied as a function of the phosphorous content as well.

Keywords Electrodeposition · Corrosion · Amorphous · Hardness, characterization · X-ray diffraction

1 Introduction

Numerous studies have been carried out on deposition of ternary NiCoP thin films, primarily due to their potential applications in high density recording [1–4], microelectromechanical systems [5–7], batteries [8, 9] and other engineering areas. These alloys exhibit unique magnetic [10, 11], wear resistant [12], heat conductive [13, 14] and electrocatalytic properties [15, 16]. Electrodeposition and electroless deposition techniques are usually preferred over more expensive and high maintenance vacuum processes due to their ability to tailor the deposit structure and properties at low operating temperatures. Electrodeposited amorphous alloys are generally more porous, less uniform and less corrosion resistant than their electroless counterparts [17]. However, due to the ease of operation, lower cost, faster deposition rates and stable baths [17], electrodeposition is preferable for most applications.

A number of electrodeposition studies of NiCoP deposition are reported [18–25]. Electrodeposition of these alloys is of special interest since they exhibit two types of phenomena—anomalous deposition and induced deposition [26]. In anomalous deposition, the less noble metal deposits preferentially, and consequently, its content in the alloy is much higher than its relative content in the solution. In induced deposition, metalloids such as P and B are deposited in the presence of Ni and Co although they cannot be deposited alone. Since the properties of these alloys are greatly affected by their atomic content as well as the structure, the effect of various process variables on the atomic content and structure is an important issue for their wide application. Djokic [18] used a phosphorous acid bath to study the effect of current density on the deposit atomic content. He found that increasing the current density enhanced the Co content in the electrodeposit, while that of Ni and P decreased. Park et al. [27] observed that increasing the Co content in the solution resulted in an increase in the relative Co content in the deposit. However, the current efficiencies were found to remain essentially constant. In addition, the phosphorous (P) content in the deposit was found to increase with the hypophosphite (source of P) concentration in the electrolytic bath. The morphology and the structure of the deposits were also found to be dependent on the P content. In general, the

✉ Shashi B. Lalvani, lalvansb@miamioh.edu | [1]Department of Mechanical Engineering and Energy Processes, Southern Illinois University, Carbondale, IL 62901, USA. [2]Department of Chemical Engineering, University of Louisville, Louisville, KY, USA. [3]Department of Chemical, Paper and Biomedical Engineering, Miami University, Oxford, OH, USA.

Published online: 05 December 2020

incorporation of phosphorous and its relative content in the alloy deposit leads to the production of amorphous alloys [26]. In a recent study, Huang et al. [28] grew porous NiCoP films on Ni foam using molten-salt electrolytes for asymmetric supercapacitors. Liu et al. [29] have obtained Co-Ni-P deposits with enhanced wear properties using supercritical CO_2 emulsion. Lew et al. [30] have studied the effect of pH and current density in electrodeposited thin alloy films. Ma et al. [31] have investigated anti-wear properties of Co-Ni-P electrodeposited coatings. In most of the studies, the phosphorous source used has consistently been hypophosphite. The impact of oxyacids (H_3PO_4, H_3PO_3) as a phosphorous source and the impact on the deposition and coating characteristics has not been sufficiently discussed in the literature.

The purpose of the present work is to establish the influence of the electrodeposition process variables on the atomic content of the NiCoP amorphous deposits and the current efficiency of deposition. In addition, the influence of phosphorous acid concentration and the buffer (phosphoric acid) concentrations on the structure and atomic content of the deposits is also evaluated. Finally, the effect of the relative P content on the deposit properties such as corrosion resistance, hardness and thermal stability is presented.

2 Experimental

Electrodeposition of NiCoP was carried out using a bath (Table 1) adapted from the study conducted by Djokic [18]. All the chemicals were obtained from Fisher Scientific (Chicago, IL). The electroplating baths were prepared with distilled, deionized water and reagent grade chemicals. Hydrochloric acid and sodium hydroxide solutions were used for pH adjustments. Electrodeposition was carried out in a 3-electrode electrochemical cell. The working electrode (circular copper foil with an exposed surface of 15 mm diameter) was a rotating disc electrode (RDE) so as to ensure well defined hydrodynamic condition and uniform deposition. The copper foils were polished with SiC paper. The substrates were then degreased with acetone prior to deposition. A platinum mesh was used as a counter electrode while the reference electrode used was a saturated calomel electrode (SCE). Unless otherwise noted, electrodeposition was carried out galvanostatically at 350 mA/cm^2 at a temperature of 80 °C. The initial pH of the bath (unless specified) was kept at 1.0.

Table 1 Bath Composition used for electrodeposition of Ni-Co-P, Ni-P and Co-P

Component	Bath composition for three deposits		
	Ni-Co-P	Ni-P	Co-P
$NiSO_4.6H_2O$	80 **(g/l)**	80 **(g/l)**	
$NiCl_2.6H_2O$	30 **(g/l)**	30 **(g/l)**	
$CoSO_4.6H_2O$	70 **(g/l)**		70 **(g/l)**
$CoCl_2.6H_2O$	15 **(g/l)**		15 **(g/l)**
H_3PO_3	25 **(g/l)**	25 **(g/l)**	25 **(g/l)**
H_3PO_4	40 **(g/l)**	40 **(g/l)**	40 **(g/l)**

g/l stands for grams per liter

The deposit corrosion rate was determined by the potentiodynamic polarization technique using a Gamry P3 potentiostat/galvanostat. The alloy atomic content was determined using energy dispersive X-ray spectroscopic (EDS) analysis similar to the procedure followed by Lew et al. [30]. The structure of the alloys, determined by X-ray diffraction (XRD) was performed in a 2 θ angle range of 20–90°. A copper target was used with a diffracted beam monochromatometer. The surface morphology of the unetched surface was examined using scanning electron microscopy (SEM). The recrystallization of electrodeposits at elevated temperatures was examined by differential scanning calorimetry (DSC). Chemical bonding information was obtained via x-ray photoelectron spectroscopy (XPS). The thickness of the deposits used for instrumental analysis was about 50 µm.

3 Results and discussion

Figure 1 contains cyclic voltammograms representing the deposition of NiP, CoP and NiCoP. It was observed that Ni and Co deposition appears to involve a single reduction step. The various individual electron transfer processes are not discernible for the scan rates used in this study. It is observed from Fig. 1 that the cathodic peaks for the three depositions are very similar in shape with the difference only being in the magnitude of the deposition peak currents. The deposition peak currents were found to be increasing in the order of NiP<CoP<NiCoP, similar to the trends reported in literature [30]. It should be noted that an increase in the deposition current is indicative of higher deposition kinetics. The reduction and subsequent deposition of Co and Ni occurs at potentials of −490 and −475 mV vs. SCE, which are fairly close to one another. The theoretical half-cell potentials for Co and Ni deposition are 551 and 519 mV vs SCE, respectively. The cyclic voltammograms also provided information regarding the oxidation and dissolution of the deposited layers. Oxidation of the metals (Ni) occurred in two steps: Ni^o to Ni^+ (−450 mV vs. SCE), and its subsequent conversion to Ni^{2+} (−290 mV vs. SCE). A two-step oxidation mechanism was also observed for Co. The current peak heights are found to be proportional to

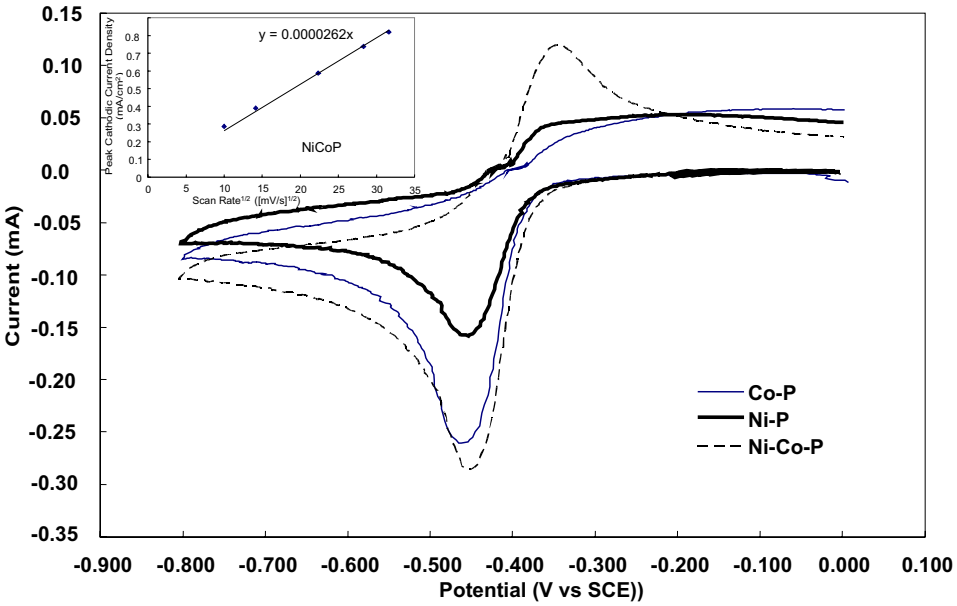

Fig. 1 Cyclic voltammetric profiles of Co-P, Ni-P, and Ni-Co-P deposition

the square root of the scan rates (inset in Fig. 1) indicative of reversible reactions of freely diffusing species and not dependent on surface adsorbed species.

As mentioned earlier, both anomalous and induced deposition have been observed to occur during metal-metalloid (M-P) electrodeposition. The following electrochemical reactions [18, 26, 28–33] relevant to the electrodeposition of the metal-phosphorous alloys need to be considered for M-P formation:

$$H^+ + e^- \rightarrow H_{ads} \tag{1}$$

$$H_3PO_3 + 2H^+ + 2e^- \leftrightarrow H_3PO_2 + H_2O \tag{2}$$

$$H_3PO_3 + 3H^+ + 3e^- \leftrightarrow P_{ads} + 3H_2O \tag{3}$$

$$H_3PO_2 + H^+ + e^- \leftrightarrow P + 2H_2O \tag{4}$$

$$HPO_3^{2-} + 2H_2O + 3e^- \leftrightarrow P + 5OH^- \tag{5}$$

$$H_3PO_3 + 6H_{ads} \rightarrow PH_3 + 3H_2O \tag{6}$$

$$2PH_3 + 3M^{2+} \rightarrow 3M^o + 2P^o + 6H^+ \text{ (induced deposition)} \tag{7}$$

$$M^{2+} + 2e^- \rightarrow \frac{M^o}{M_{ads}} \text{ (cathodic reduction)} \tag{8}$$

$$M_{ads} + P_{ads} \rightarrow M - P_{phase} \tag{9}$$

where M and P represent the metal atoms and phosphorous atoms, respectively.

Ratzker et al. [34] and Ohno et al. [35] were the earliest to describe mechanisms for Ni-P deposition. Ratzker et al. [34] proposed a mechanism for the induced metalloid addition to the electrodeposited alloy based on PH_3 formation in the electrolyte (reactions 1, 6 and 7). The occurrence of phosphine during Ni-P deposition has been confirmed by other researchers [36, 37]. On the other hand, Ohno et al. [35] proposed a concept of P atoms formed by the reduction of H_3PO_3 (–0.773 V vs SCE) and the incorporation of the P adsorbed atoms into the lattice metal lattice (Reactions 3, 8 and 9). The latter step was considered the rate limiting step. The electroreduction of H_3PO_3 is not clearly seen in cyclic voltammogram. However, it is likely that the observed broad peak is a composite of several peaks representing other elementary electrochemical reactions. Nonetheless, according to either mechanism (suggested by [33] or [34]), there is a need to maintain a high concentration of H_3PO_3 and H^+ near the surface of the electrode, which is possible in this investigation due to the low solution pH. Thus, we hypothesize that both mechanisms as given by reactions (1), (6), (7) and reactions (3), (8) and (9), respectively, may be responsible for the metalloid incorporation into the deposits.

3.1 Effect of stirring rate

The influence of the rotational speed (ω) of the RDE on the atomic content of the alloy produced and the current efficiency is shown in Fig. 2. The applied current density was 350 mA/cm^2 and the bath was maintained at 80 °C. It is observed that the phosphorous content increases from 9 to 19.8 at. % as ω is increased from 0 to 1500 rpm. The effect of this increased mass transport rates is most

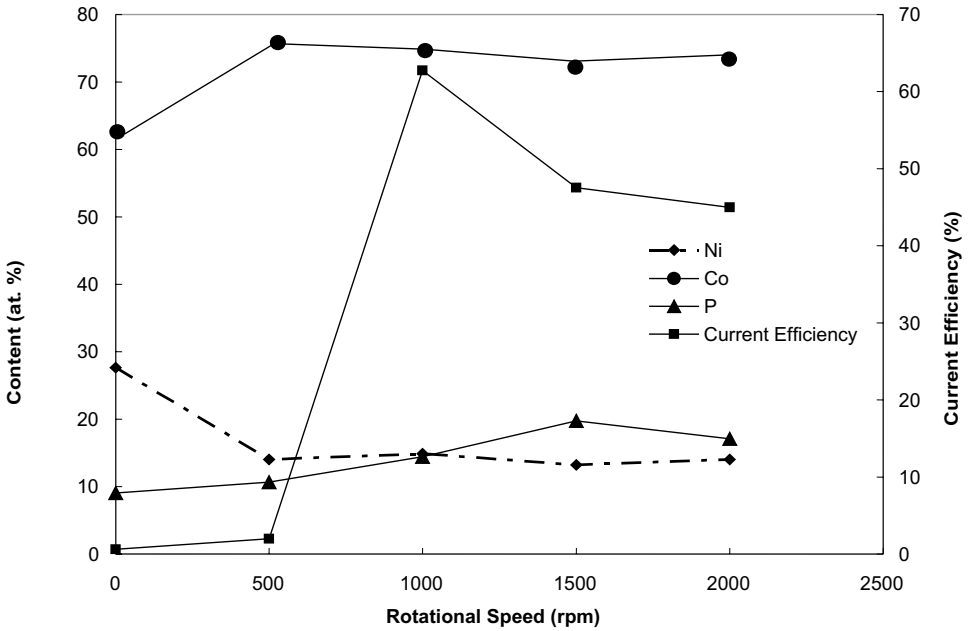

Fig. 2 Elemental content and current efficiency as a function of rotational speed (350 mA/cm^2, 80 °C, pH = 1) for electrodeposited Ni-Co-P coatings

prominent in the case of phosphorous deposition (>100% increase). The current efficiencies were also significantly enhanced (0.61–62.7%) as a result of increased convection when ω is increased from 0 to 1000 rpm. The diffusivity of H^+ (~10^{-8} m^2/s) is significantly higher than those of Co^{2+} (~10^{-10} m^2/s) and Ni^{2+} (~10^{-10} m^2/s) [38–40]. Hence, at low rotational speeds (ω), H^+ diffusion and its reduction at the electrode leads to significant hydrogen evolution (reaction 1). This results in a corresponding decrease in the current efficiency. It must be noted that an enhancement in rotational speed results in a corresponding greater increase in the mass transfer rates of Ni^{2+} and Co^{2+} as compared to the corresponding increase of H^+ transport rate. Thus, an enhanced fraction of the applied current is utilized for the deposition of the metals (reaction 8) resulting in the observed increase in current efficiency. However, the absolute hydrogen evolution rate is expected to increase with stirring. At higher stirring rates (>1000 rpm), the differences in the mass transport rates of the metal ions and that of hydrogen is significantly diminished, thereby leading to loss in current efficiency. In addition, the phosphorous content is observed to increase. The incorporation of phosphorous is expected to be obtained from phosphine (reaction 7) and thus an increase in phosphorous content corresponds to an increase in the formation of phosphine. However, past researchers have noted the evolution of phosphine during electrodeposition. Thus, loss of phosphine will also result in an additional decrease in the current efficiency and would partly explain the decrease in efficiency at stirring rates greater than 1000 rpm. The rotational speed of the RDE was maintained at 1500 rpm for all subsequent experiments.

The data (Fig. 2) show that Co: Ni atomic ratio in the deposits ranges from 1.6 to 5.1 which is significantly larger than the corresponding ratio present in the deposition bath (0.77). This phenomenon is a result of anomalous deposition [26]. Even though the reaction conditions involve low pH, the following reactions may occur due to the rapid depletion of H^+ ions near the electrode-electrolyte interface, thereby creating a local increase in the OH^- ion.

$$M^{2+} + OH^- \leftrightarrow M(OH)^+ \tag{10}$$

$$M(OH)^+ \rightarrow M(OH)^+_{ads} \text{ (due to electrostatic force of the cathode)} \tag{11}$$

$$M(OH)^+_{ads} + 2e^- \leftrightarrow M + OH^- \tag{12}$$

Additional OH^- ions may also be produced by the following reaction

$$H_2PO_2^- + e^- \leftrightarrow P + 2OH^- \tag{13}$$

Similar findings were reported in the literature [41, 42] wherein the Co content was significantly concentrated in the deposits as compared to the precursor bath due to the differences in the adsorption rate of the $M(OH)^+_{ads}$ species in spite of the acidic medium.

Since the adsorption ability of $Co(OH)^+$ has been reported [41, 42] to be higher than that of $Ni(OH)^+$ [32, 33], Co is enriched within these alloys by reactions (11) and (12). The OH^- formation by reaction (12) and the elemental phosphorous formation reactions (reactions 5 and 13) favor further formation and enhanced adsorption of Co

$(OH)^+$ at the electrode surface. At low ω, the Co enrichment in the deposit due to Co $(OH)^+$ formation and adsorption, is not as significant due to two factors. First, the overall metal concentration near the electrode surface is small on account of relatively high mass transfer resistance. Second, at low rotational speeds, low rate of phosphorous deposition (due to small phosphorous acid concentration at the interface) results in a small increase in OH^- content at the electrode. As more phosphorous is deposited (on increasing ω), the OH^- concentration near the electrode also increases resulting in the Co enrichment in the deposit.

3.2 Effect of current density

The effect of current density on the atomic content and current efficiency is shown in Fig. 3. The stirring rate and bath temperature for these experiments were kept at 1500 rpm and 80 °C, respectively. Electrodeposition of NiCoP was conducted at current densities of 0.05, 0.15, 0.25 and 0.35 A/cm^2 for 30 min. The data in Fig. 3 show that the phosphorous content decreased from 19.9 at. % to 14.3 at. % as the current density was increased from 0.05 to 0.35 mA/cm^2. The data agree well with that reported by the previous researchers [42]. An increase in the current density leads to a corresponding increase in the partial current for hydrogen evolution rather than the formation of H_{ads} on the electrode surface leading to a decrease in phosphine formation (reaction 8) and, therefore, concomitant decrease in phosphorous content. The local increase in pH due to hydrogen evolution also suppresses elemental phosphorous (reactions 3, 4, 5, and 13) and phosphine formation (reaction 6) near the electrode-electrolyte interface. It should be noted that for either mechanism, reactions (3) and (6) require the presence of H_3PO_3 species. The increase in hydrogen evolution would result in the dissociation of H_3PO_3, thereby decreasing the forward rates of reactions as shown by Eqs. (3) and (6) and thus, lowering the rates of reactions given in (7) and (9). As a result, the phosphorous content in the electrodeposited alloy decreases. The Co:Ni molar ratio in the plating bath (Table 1) was 0.77. When a current density of 0.05 A/cm^2 was impressed, the Co:Ni ratio in the deposit was found to be 0.68. On increasing the applied current density to 0.15 A/cm^2, the ratio increased to 3.49. The Co:Ni molar ratio was found to be 3.75 with a further increase in the current density to 0.35 A/cm^2. The pH at the electrode surface increases due to hydrogen evolution and as a result, Co is enriched in the deposit. The results are consistent with the findings reported by Djokic [18].

The current efficiency, on the other hand, is observed to increase from 34.6% to 54.6%. In general, an increase in current density results in a decrease in current efficiency of deposition due to an increase in the parasitic hydrogen evolution. However, since the potentials at which Ni, Co and P deposit are generally more negative than the potential for hydrogen evolution, an increase in current (with a corresponding increase in the applied potential) is expected to favor the deposition reactions under mass transport controlled conditions. This aspect is further exaggerated due to the complex mechanism underlying deposition, induced deposition (via the formation of phosphine and/or electrodreduced H_3PO_3 to P_{ads}), and anomalous deposition due to higher OH^- local concentration at the interface due to faster kinetics of several reactions.

3.3 Effect of pH

An examination of reactions (1)–(13) shows that the solution pH is an important process parameter, both, with respect to the atomic content of the alloy and

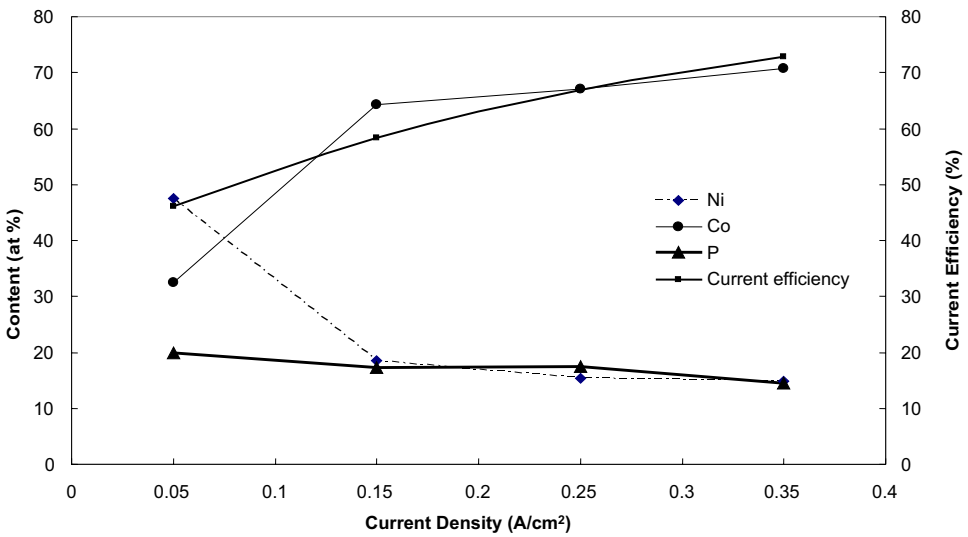

Fig. 3 Elemental content and current efficiency as a function of applied current density (1500 rpm, 80 °C, pH = 1) for electrodeposited Ni-Co-P coatings

the current efficiency, since it controls the concentration of the species undergoing reduction and the supply of protons for the parasitic hydrogen evolution. In this study, experiments were conducted using baths maintained at four different pH values ranging from 0.7 to 1.75. Phosphorous content was observed to decrease from 20.5 at % to 12 at % with increasing pH. The decrease in the phosphorous content with the bath pH (Fig. 4) can be explained by either of the proposed mechanisms which clearly show that more acidic baths will promote the incorporation of the metalloid. These results contrast with those reported by Lew et al. [30] wherein phosphorous content increased (2.98% to 9.82%) with increasing pH (1.5 to 5). A primary difference between the two studies is that the Lew et al. produced crystalline NiCoP via direct deposition method resulting in much lower P inclusion vs indirect deposition dominating in this study. The higher pH (initial) also results in the enhancement of the underpotential deposition of Co, and, thus leads to an increase in the current efficiency and enrichment of Co in the film. The hydrogen evolution reaction is significantly arrested by the ten-fold decrease in the proton concentration in the bulk solution resulting in a nearly ninefold increase in efficiency. In accordance with reactions (10)–(12), the Co:Ni atomic ratio in the deposits showed a 77% increase with an increase in pH from 0.7 to 1.4, similar to what has been reported in the literature. A further increase in the bulk pH resulted in a 28% decrease in the Co:Ni ratio.

3.4 Effect of temperature

Electrodeposition of NiCoP was conducted from a plating bath of initial pH of 1.0 at various temperatures and 0.35 A/cm^2. Very poor-quality electrodeposits were obtained at temperatures lower than 60 °C and are not reported. When electrodeposition was carried out at a 60 °C, the phosphorous and nickel contents of the electrodeposited alloy were 15.2 and 5.67 at. %, respectively (Fig. 5). The current efficiency was calculated to be 28.2%. No significant change in the phosphorous content was observed when the temperature was elevated. However, the nickel content is observed to increase with temperature. When electrodeposition was carried out at 90 °C, the nickel content was observed to be 23.2 at. %. As mentioned earlier, the electrodeposition process appears to be mass transfer controlled. On increasing the temperature, the resistance to mass transport decreases, and as a result, the electrode reaction kinetics becomes the rate controlling step. Therefore, the reduction of nickel is favored over that of P reduction. The current efficiency was also found to increase with temperature. On increasing the bath temperature from 60 to 90 °C, the current efficiency increased nearly three-fold to 83.5 at. %. The mass transport rate of all the species increases with temperature and the relative Co^{2+}, Ni^{2+} and H_3PO_3 contents at the electrode also increase are mass transfer limited in comparison to H^+ transport rate. Thus, the relative amount of hydrogen evolution decreases and hence, the observed increase in the current efficiency.

Thus, it can be concluded that by varying the process variables, namely, temperature, pH, the applied current

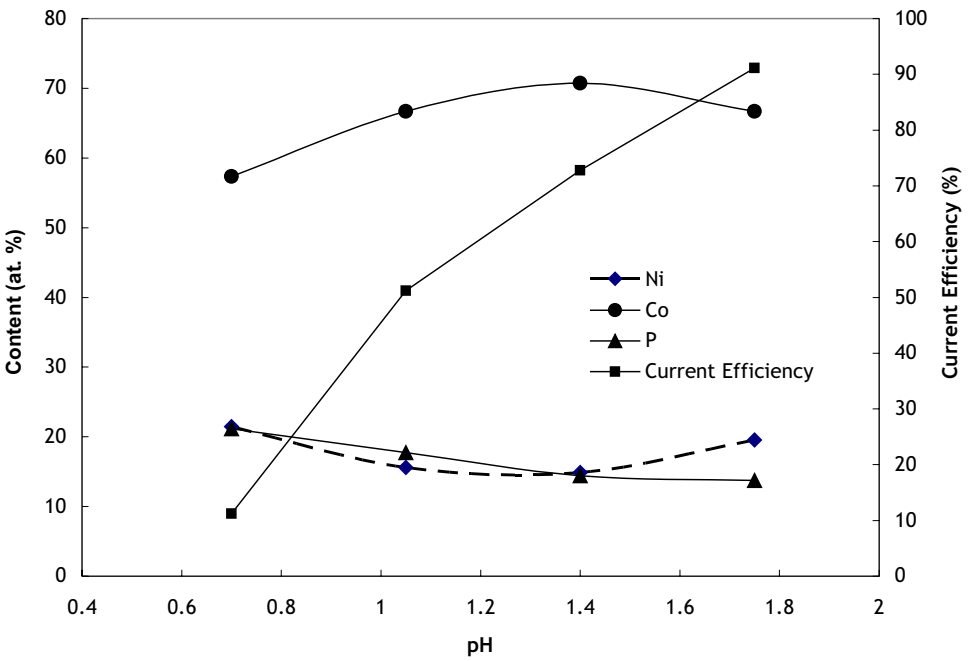

Fig. 4 Elemental content and current efficiency as a function of pH (1500 rpm, 80 °C, 350 mA/cm^2) for electrodeposited Ni-Co-P coatings

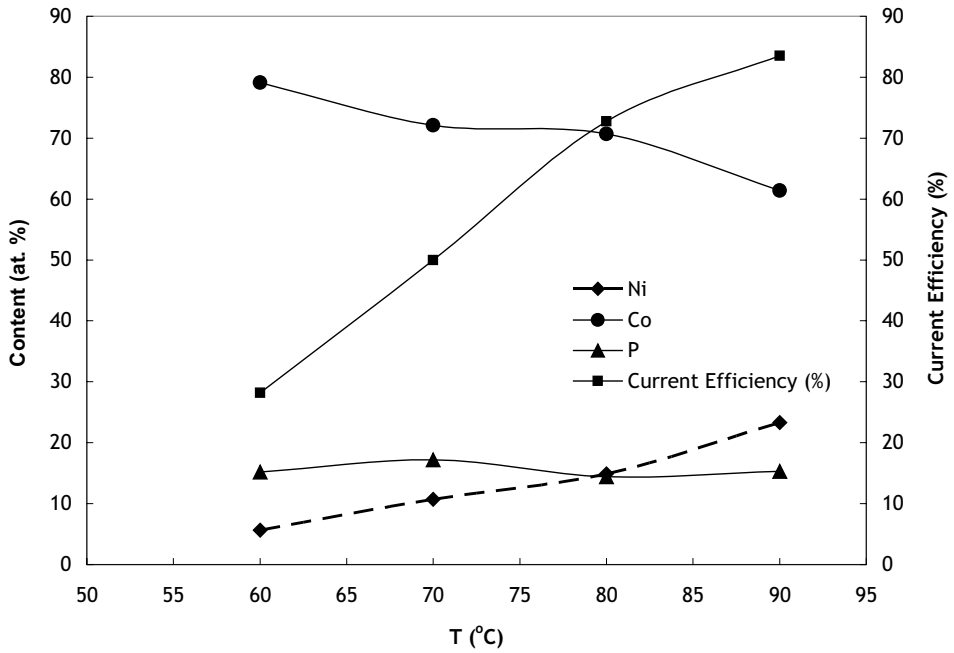

Fig. 5 Elemental content and current efficiency as a function of temperature (1500 rpm, 350 mA/cm^2, pH = 1) for electrodeposited Ni-Co-P coatings

density and the stirring rate, the atomic content of the electrodeposit from any given bath can be tuned.

3.5 Bath composition

The effect of phosphoric acid (buffering agent) and phosphorous acid (P precursor) concentrations on the deposit characteristics is shown in Figs. 6 and 7. The use of phosphoric acid did not change the atomic content of the deposits obtained. However, its inclusion (at 40 g/L) in the plating bath resulted in smoother deposits (Fig. 6b) as compared to the deposits obtained in the absence of a buffering agent (Fig. 6a).

Increasing the phosphorous acid content in the plating bath from 0 to 35 g/L resulted in an increase in the phosphorous content of the alloy from 0 to 24.9 at. % in the deposits accompanied by a 45% decrease in the current efficiency (Fig. 7). It must be noted that the increase in phosphorous content generally results in lowered efficiencies presumably due to the lower conversion efficiency of phosphine/direct reduction of adsorbed H_3PO_3 to phosphorous deposits. A further increase in the phosphorous acid concentration to 50 g/L resulted in only a slight increase in the phosphorous content in the deposit to 23 at. %. The relative Ni content in the deposit also remained relatively fairly constant. However, the relative Co content in the deposit decreased to about 50% when phosphorous

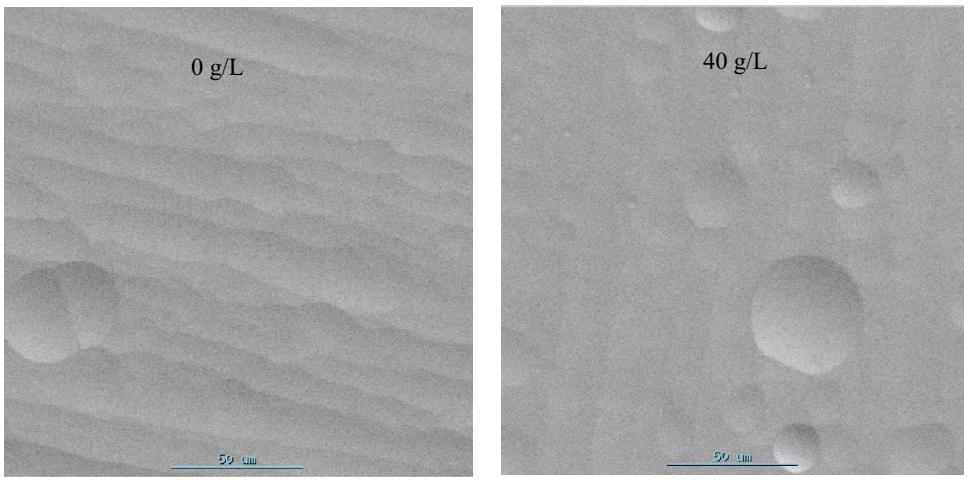

Fig. 6 SEM images of NiCoP electrodeposits from a bath containing (**a**) no phosphoric acid and (**b**) 40 g/L of phosphoric acid

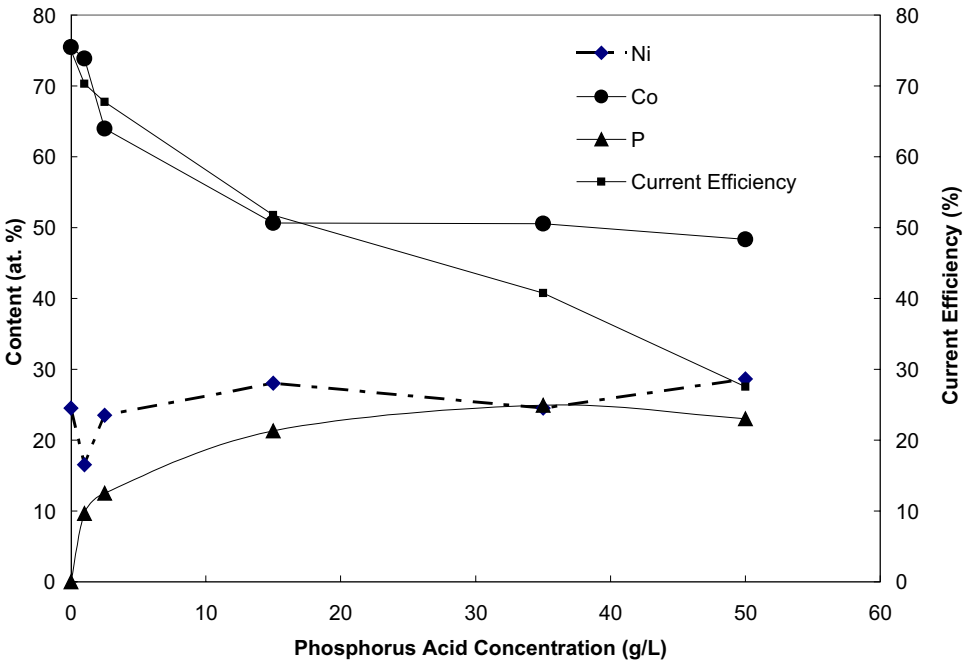

Fig. 7 Elemental content and current efficiency as a function of phosphorous acid concentration in the electrolyte (1500 rpm, 80 °C, pH = 1, 350 mA/cm^2) for electrodeposited Ni-Co-P coatings

acid concentration in the bath was increased to 15 g/L. Further increase in the phosphorous acid content in the bath did not affect the Co content in the deposit. The current efficiency of NiCo deposition was calculated to be 75%. In contrast, the current efficiency of NiCoP deposition from an electrolyte containing 50 g/L phosphorous acid was only 27.5%.

3.6 Deposit characteristics

A number of electrodeposits (not shown) characterized by scanning electron microscopy at a magnification of 500 were found to be fairly smooth. The polishing of the substrate prior to electrodeposition resulted in the formation of some straight and parallel markings. The deposits also showed the presence of these markings which is indicative of uniform deposition. Thus, the alloy can be used to deposit into crevices and around sharp corners. It was also observed that increasing the current density resulted in smoother deposits. The electrodeposits obtained from baths maintained at a low pH were columnar. Upon increasing the pH of the bath, smoother deposits were obtained.

The x-ray diffraction spectroscopy (Fig. 8) data indicates that a major portion of the electrodeposits is mainly amorphous in nature. As identified in the figure, the broad hump appearing at between 2θ value of 40° and 50 ° corresponds to the amorphous NiCoP alloy. The sample prepared from a solution devoid of the P precursor (0% P sample) showed a monophasic NiCo alloy and has a distinguishable diffraction peak at 41.1°. The sample has a hexagonal symmetry, specifically exhibiting the {0 1 0} plane. The broad hump becomes broader as the P content in the sample increases. The coating also exhibited an FCC structure, specifically {200} plane. This could be related to the Cu substrate. It has been concluded by past researchers [27, 43] that low pH promotes the FCC structure in NiCoP. The XRD patterns reported in this paper agree with those reported by Djocik [18]. X-ray photoelectron spectroscopy (XPS) was employed to evaluate the atomic content and valence states of $Ni_{23}Co_{61}P_{16}$ (Fig. 9), whose XRD spectrum was not determined. The figure clearly shows the coexistence of Co, Ni and P elements along with some amount of O (presumably due to exposure to air) which is in accordance with the XRD results of samples reported in Fig. 8. The Ni^{2+} peak is located at a binding energy of 868 eV. The Co 2p peak is observed at a binding energy of 789 eV. The P 2p peaks are observed at 130.4 and129.3 eV. The O 1 s peak is obtained at 531 eV. The data show the presence of elemental phosphorous and it does not exist either as phosphate or phosphide.

Figure 10 shows the non-isothermal DSC thermogram of the NiCoP electrodeposits. The number of phases formed varied with the phosphorous content in the electrodeposits. While there are no exothermic peaks for the NiCo electrodeposit, it is observed that the number of exothermic peaks between 300 and 400 °C increased with phosphorous content (one for 15 at. % P and two for 21 at. % P). In addition, two exothermic peaks were observed at temperatures greater than 400 °C for the deposit with 15 at. % P, while a single broad peak was observed for the deposit with 21 at. % P. The DSC thermogram showed only

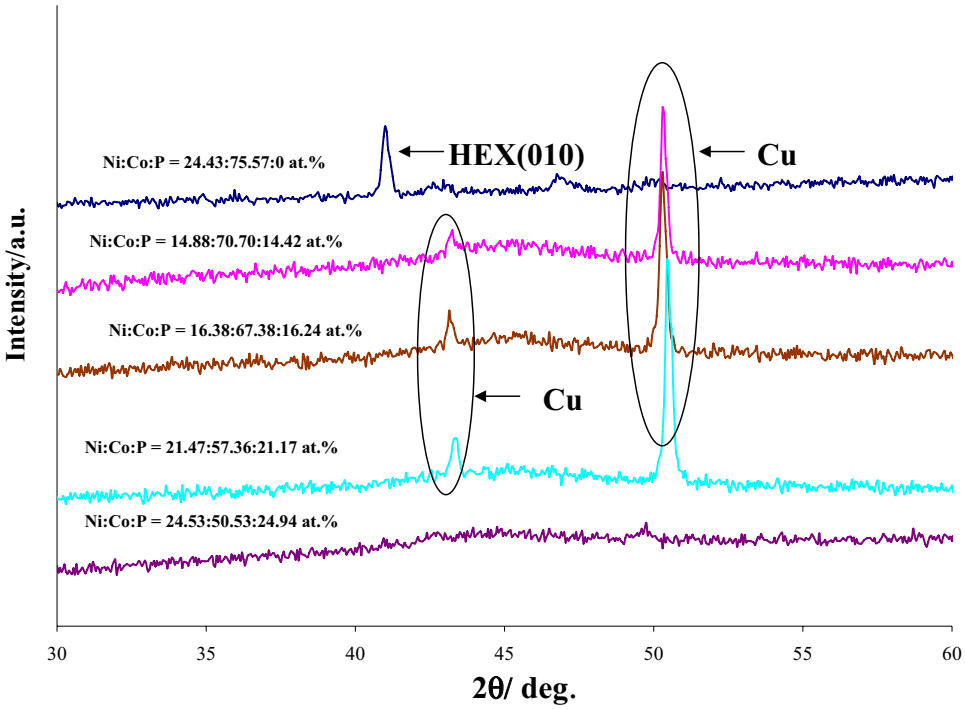

Fig. 8 XRD patterns of electrodeposited Ni-Co-P films at various P contents in the deposits

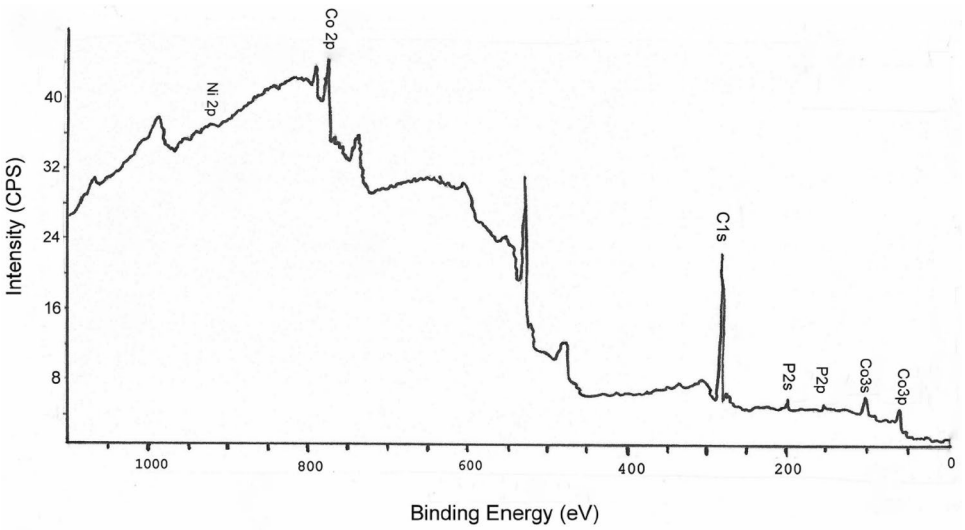

Fig. 9 XPS spectra of $Ni_{23}Co_{61}P_{16}$

one endothermic peak for the deposit with no phosphorous. The small exotherm observed for the deposit with 21 at. % P represents the precipitation of fine Co particles in the amorphous matrix [18]. The data show that the exothermic peak begins to appear at 340 °C and the peak is observed at 380 °C. This corresponds to the devitrification of the remaining amorphous phase to form Co_xP_y and Ni_xP_y compounds [18]. The broad peak at higher temperatures (>420 °C) is related to the decomposition of Co_xP_y and Ni_xP_y to Ni, Co, Ni_3P and Co_2P [18]. The deposit containing 15 at. % P exhibited broad exothermic peaks at 330 °C and two small peaks at 450 and 500 °C. The wide exothermic peaks in the DSC thermograms indicate the structural relaxation of the amorphous phase. The endothermic peak of the NiCo electrodeposit at 480 °C corresponds to the one observed for pure Co electrodeposit.

The data on the effect of phosphorous content on the corrosion properties of the electrodeposited NiCoP alloy in simulated sea water (33 g/L NaCl solution) are provided in Table 2. The data show that the corrosion rate of the bimetallic alloy (no metalloid) is 0.77 µm/year. The inclusion of metalloid, P, in the alloy was found to significantly reduce the corrosion rate [44]. For example, when the phosphorous content in the alloy is 23 at. %, the corrosion rate was

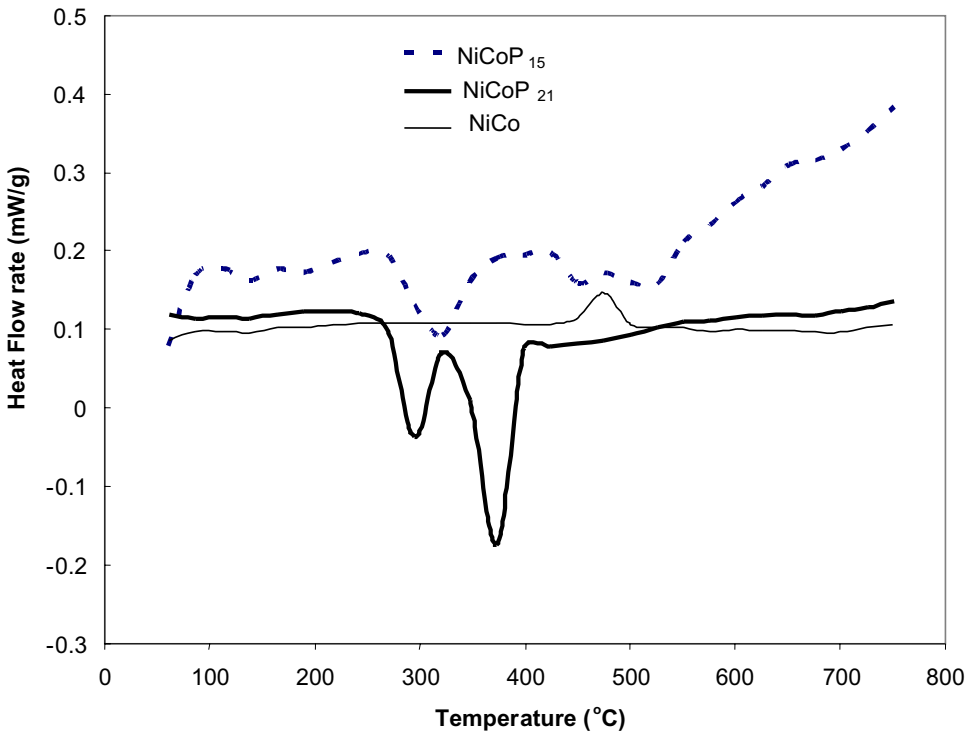

Fig. 10 DSC profiles of Ni-Co-P deposits with 0%, 15% and 21% P content in the deposits

Table 2 Corrosion data of Ni-Co-P deposits as a function of phosphorous content

at. % P in deposit	E_{corr} mV vs. SCE	I_{corr} A	Corr rate mm/year ($\times 10^{-3}$)
0	−867.8	2.51×10^{-06}	0.768
9.93	−829.2	1.00×10^{-06}	0.306
23.02	−757.5	0.29×10^{-06}	0.088

calculated to be 0.09 µm/year. The corrosion potentials shifted to more positive potentials with the increase in phosphorous content. The shift was greater than 100 mV when the phosphorous content was increased from 0 to 23 at. %. The non-crystalline structure and the presence of the metalloid, P, led to the absence of grain boundaries and thus the exhibition of exceptional corrosion resistance.

Figure 11 contains the data on the Knoops Hardness (HK) of the NiCoP electrodeposits as a function of the

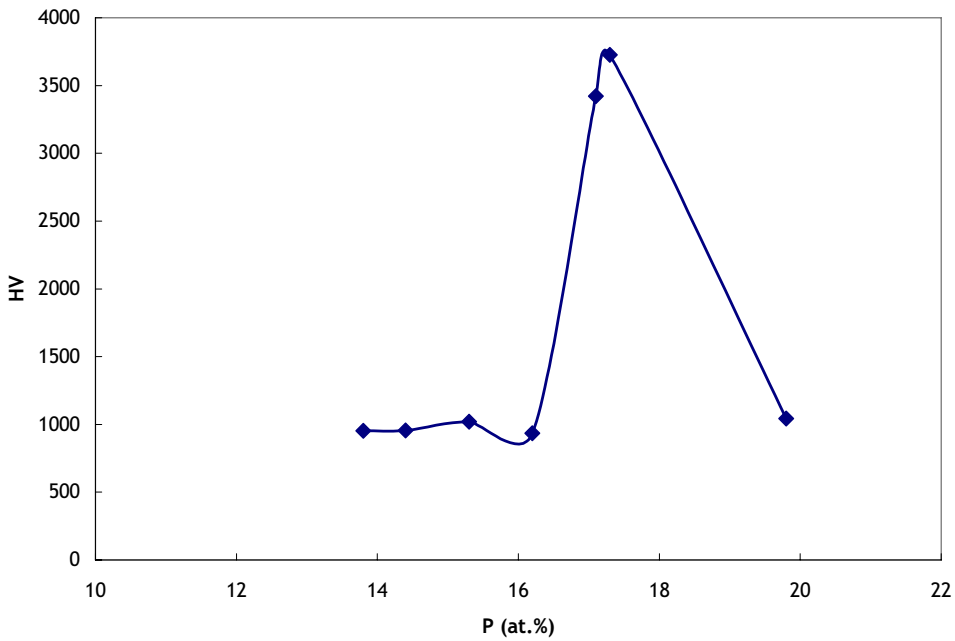

Fig. 11 Knoop hardness of Ni-Co-P electrodeposits as a function of the P content in the coatings

phosphorous content. The coatings used were around 50 µm thick and thus the impact of the softer copper foils was negligible. At P contents less than 16%, the HK values were approximately 1000 which is higher than those reported in literature for NiCoP alloys [45]. Furthermore, it is observed that a slight increase in the phosphorous content from 16.2 to 17.3 at. % led to a 290% enhancement in the HK from 954 to 3723. A further increase in the phosphorous content to 19 at. % resulted in a drop in the hardness of the deposit. The formation of micro/nano-crystalline phases in this range of P content (16–17 at. %) is probably the reason for this sudden increase in the hardness of the deposit. However, on a further increase in the relative P content, the deposit becomes increasingly amorphous and as a result the hardness of the deposit decreases. Similar observations were made with respect to NiP deposits where the hardness value was observed to decrease with increasing phosphorous content greater than 11 at. %.

4 Summary

The effect of the various deposition parameters on the alloy atomic content of the NiCoP deposits obtained from oxyacid (H_3PO_3/H_3PO_4) based P source has been discussed in detail. Current density and the pH of the precursor solution is critical for tuning the P content in the deposit. The atomic content of the electrodeposits can be further modulated by bath composition and temperature of the electrolyte. Phosphorous content determines the amorphous nature of the deposits. XRD, XPS and DSC data show the amorphous nature of NiCoP deposits. The deposits show exceptional corrosion resistance and hardness. The corrosion resistance and the Knoop hardness are observed to be strong functions of the phosphorous content. Heating of the deposits results in change of the amorphous phase to crystalline.

Funding Funding for this research was provided by the Consortium of Advanced Radiation Sources, Illinois and Materials Technology Center, SIU.

Compliance with ethical standards

Conflict of interest The author(s) declare that they have no competing interests.

References

1. Nakamura Y (1999) Perpendicular magnetic recording – progress and prospects. J Magn Magn Mat 200:634
2. Homma T, Kita Y, Osaka T (2000) Microstructural study on the functionally graded magnetic thin films prepared by electroless deposition. J Electrochem Soc 147(1):160
3. Homma T, Shiowkawa J, Sezai Y, Osaka T (1996) In situ analysis of the deposition process of electroless CONiP perpendicular magnetic recording media. Proc Electrochem Soc, PV 95–18:181
4. Homma T, Inoue K, Asai H, Ohrui K, Osaka T (1991) Microstructural study of electorless-plated CONiP ternary alloy films for perpendicular magnetic recording media. IEEE Trans Magn 27(6):4909
5. Chin T-S (2000) Permanent magnet films for applications in microelectromechanical systems. J Magn Magn Mat 209:75
6. Judy JW, Muller RS (1997) Magnetically actuated, addressable microstructure. J Microelectromech Syst 6(3):249
7. Judy JW, Muller RS, Zappe HH (1995) Magnetic microactuation of polysilicon flexure structures. J Microelectromech Syst 4(4):162
8. Maurel F, Knosp B, Backhaus-Ricoult M (2000) Characterization of corrosion products of AB5-type hydrogen storage alloys for nickel-metal hydride batteries. J Electrochem Soc 147:78
9. Wang CC, Goto KS, Akbar SA (1991) Demixing of (Ni, Co) O under an oxygen potential gradient using a YSZ-based galvanic cell. J Electrochem Soc 138:3673
10. Passal F (1966) Bath and process for the electrodeposition of nickel and nickel-cobalt alloys, US Patent 3,274079
11. Friemel F (1966) Chem Abstr 67(1967) 17376h, East German Patent 52,869
12. Jato M. Japanese Patent, Chem. Asbstr. 82 (1975) 91774n, 74, 33723
13. Ichioka S, Koda T (1975) Japanese Patent, Chem. Asbstr. 83 (1975) 87387s, 75,02377
14. Singh VB, Singh VN (1976) Electrodeposition of nickel-cobalt alloys from an acetate bath. Plat Sur Fin 63(7):34
15. Hu C-C, Weng C-Y (2000) Hydrogn evolving activity on nickel-molybdenum deposits using experimental strategies. J Appl Electrochem 30:499
16. Hu C-C, Bai A (2001) Optimization of hydrogen evolving activity on nickel-phosphorus deposits using experimental strategies. J Appl Electrochem 31:565
17. Schwartz M (1994) In: Bunshah RF (ed) Handbook of deposition technologies for films and coatings, 2nd edn. Noyes Publ, Parkridge, NJ, pp 524–531
18. Djokic SS (1999) Electrodeposition of amorphous alloys based on the iron group of metals. J Electrochem Soc 146(5):1824–1828
19. Parente MMV, Mattos OR, Diaz SL, Lima Neto P, Fabri Miranda F (2000) Electrochemical characterization of Ni-P and Ni-Co-P amorphous alloy deposits obtained by electrodeposition. J Appl Electrochem 31:677–683
20. Rivero G, Multigner M, Garcia JM, Crespo P, Hernando A (1998) Magnetic and structural properties of electrodeposited Co-Ni-P amorphous ribbons. J Magn Magn Mat 177–181:119–120
21. Yoshida K, Yamashita T, Saito M (1988) Magnetic properties and media noise of Co-Ni-P plated disks. J Appl Phys 64(1):270
22. Sheleg MU, Nemtsevich LV, Grabchikov SS, Tochitskii TA (1991) Effect of irradiation on amorphous electrodeposited CoNiP alloy films. Phys Stat Sol (a) 126:189
23. Rauch GC, Byun C, Jones ERC, Messinger C, Greggi J Jr (1992) The effect of cluster size on media noise in Co-Ni-P thin films. IEEE Trans Magn 28(5):3105
24. Byun C, Rauch GC, Young DJ, Klepper CA (1993) Effects of hypophosphite contents and surface treatment on electroplated Co-Ni-P thin films. J Appl Phys 73(10):5575
25. Fenineche F, Chaze AM, Coddet C (1996) Effect of pH and current density on the magnetic properties of electrodeposited Co-NiP alloys. Surf Coat Tech 88:264

26. Brenner A (1963) Electrodeposition of alloys, vol I. Academic Press, New York
27. Park D-Y, Myung NV, Schwartz M, Nobe K (2002) Nanostructured magnetic CoNiP electrodeposits: structure-property relationships. Electrochem Acta 47:2893–2900
28. Huang Z, Li X, Xiang X, Gao T, Zhang Y, Xiao D (2018) Porous NiCoP in situ grown on Ni foam using molten-salt electrodeposition for asymmetric supercapacitors. J Mater Chem A 6:23746–23756
29. Liu C, Su F, Liang J (2018) Fabrication of Co-Ni-P film with excellent wear and corrosion resistance by electroplating with CO_2 emulsion. Trans Nonferrous Metals Soc China 28:2489–2498
30. Lew K, Raja M, Kim T, Thanikarasan, Mahalingam T (2008) Effect of pH and current density in electrodeposited Co-Ni-P alloy thin films. Mater Chem Phys 112:249–253
31. Ma C, Wang SC, Wang LP, Walsh FC, Wood RJK (2013) The electrodeposition and characterisation of low-friction and wear-resistant Co-Ni-P coatings. Surf Coat Technol 235:495–505
32. Yin K-M (1997) Potentiostatic deposition model of iron-nickel alloys on the rotating disk electrode in the presence of organic additive. J Electrochem Soc 144:1560
33. Ramasubramanium M, Wei J-H, Popova SN, Popov BN, White RE, Yin K-M (1996) Anamoalous codeposition of Fe-Ni alloys and Fe-Ni-SiO_2 composites under potentiostatic conditions: experimental study and mathematical model. J Electrochem Soc 143:2164
34. Ratzker M, Lashmore DS, Pratt KW (1986) Electrodeposition and corrosion performance of nickel-phosphorus amorphous alloys. Plat Surf Finish 73:74
35. Ohno I, Ohfuruton H, Haruyama S (1986) Electrodeposition of Ni-P alloys with pulsating current. J Jpn Inst Met 50:1075
36. Ordine AP, Diaz SL, Margarit ICP, Barcia OE, Mattos OR (2006) Electrochemical study on Ni-P electrodeposition. Electrochim Acta 51:1480
37. Harris TM, Dang QD (1993) The mechanism of phosphorus incorporation during the electrodeposition of nickel-phosphorus alloys. J Electrochem Soc 140:81
38. Hessami S, Tobias CW (1989) A mathematical model of anomalous codeposition of nickeliron on a rotating disk electrode. J Electrochem Soc 136:3611
39. Yin K-M, Wei J-H, Fu J-R, Popov BN, Popova SN, White RE (1995) Characterization of permalloy thin films electrodeposited on Si(111) surfaces. J Appl Electrochem 25:543
40. Vaes J, Fransaer J, Celis J-P (2000) The role of metal hydroxides in NiFe deposition. J Electrochem Soc 147:3718
41. Schwekandt D'S, Aguirre MC (2015) Electrodeposition of Ni-Co alloys. Determination of properties to be used as coins. Procedia Mater Sci 8:91–100
42. Bai A, Hu C-C (2002) Effects of electroplating variables on the composition and morphology of nickel-cobalt deposits plated through means of cyclicvoltammetry. Electrochim Acta 47:3447–3456
43. Myung NV, Park DY, Yoo BY, Sumodjo PTA (2003) Development of electroplated magnetic materials for MEMS. J Magn Magn Mater 265:189
44. Carbajal JL, White RE (1988) Electrochemical production and corrosion testing of amorphous Ni-P. J Electrochem Soc 132(12):2592
45. Huang Q (2016) Electrodeposition of Amorphous Alloys: Nickel Cobalt Phosphorus and Iron Phosphorous, MS Thesis, Case Western Reserve University